ACADEMIC PRESS

Available online at www.sciencedirect.com
SCIENCE DIRECT®

Journal of Catalysis 218 (2003) 321–333

JOURNAL OF CATALYSIS

www.elsevier.com/locate/jcat

Upper bound on the yield for oxidative coupling of methane

Yee San Su, Jackie Y. Ying, and William H. Green, Jr. *

Department of Chemical Engineering, Massachusetts Institute of Technology, Cambridge, MA 02139, USA

Received 1 November 2002; revised 23 January 2003; accepted 23 January 2003

Abstract

An approach is presented for determining an upper bound on the yield of a catalytic process, which allows for variations in the catalytic chemistry. Scaling and thermodynamic arguments are used to set parameters of an elementary step surface mechanism at values resulting in optimal yields, subject only to physical constraints. Remaining unknowns are treated as independent variables and varied over a broad range. The result is a set of thermodynamically consistent mechanisms with optimal kinetics that can be incorporated into reactor-transport models to generate yield trajectories. With this approach, an upper bound on the yield for oxidative coupling of methane (OCM) was computed. Results show that even with optimal surface chemistry, limits exist on the attainable yield. Surface energetics necessary for superior OCM performance were identified and the origins of these requirements elucidated. The resulting upper bound on OCM yield under conventional, packed-bed, continuous-feed operation was found to be 28%.

Keywords: Oxidative coupling of methane; Yield; Simulation; Kinetics; Packed bed; Parameter identification

1. Introduction

A major goal of both physical chemists and chemical engineers is the design of catalysts for technologically important processes. A first step toward this goal is understanding the fundamental limits on catalyst performance—recognizing how closely our experimental catalysts approach ideal performance. Some of these limits are well-known [1], but so far there is no general method for establishing these bounds for systems with complex nonlinear kinetics. As a result, one seldom knows whether or not a process can be substantially improved by modifying the catalyst. Another important step in catalyst design is identifying which characteristics of a catalytic system (e.g., thermochemistry of the surface intermediates, reaction barrier heights, morphology, and reactor design) are most critical for a particular application. This information could then serve as a valuable guide to further experimental work.

This paper examines the conversion of methane to ethene via the oxidative coupling of methane (OCM):

$$2CH_4 + O_2 \underset{\text{catalyst}}{\rightarrow} C_2H_4 + 2H_2O.$$

A sizeable economic incentive exists for the conversion of abundant low-value light alkanes into more valuable functionalized organics (e.g., ethene) for use as polymer/chemical precursors. While strongly dependent on ethene valuation, analyses performed by the MITRE Corporation [2], SRI [3], and Gradassi and Green [4] have placed the minimum values for OCM economic feasibility at $\sim$ 16–30% yield and $>$ 80% selectivity. These economic projections typically assume industrial conditions of elevated pressures and undiluted feed streams. For simplicity and safety, however, laboratory-scale catalyst screening has focused almost exclusively on exceeding these values in a packed-bed reactor operated at atmospheric pressure with dilute feed streams. Yet even under such favorable conditions, none of the numerous OCM catalysts synthesized since Keller and Bhasin's initial report [5] have managed to be commercially viable. This hints at some fundamental limitation on OCM yields. Alternative reactor/separation schemes have successfully been shown to exceed the yield/conversion targets and may ultimately represent the only viable future for OCM [6,7]. But before more elaborate and costly reactor schemes are pursued, the upper limit on yield for a conventional packed-bed, single-pass, continuous-feed operation needs to be fully assessed.

The notion of establishing an upper bound on OCM performance has been previously explored. At the core of many

* Corresponding author.
E-mail address: whgreen@mit.edu (W.H. Green, Jr.).

0021-9517/03/$ – see front matter
doi:10.1016/S0021-9517(03)00043-5

of these efforts is the development of an elementary-step surface mechanism. Upon acquisition of experimental data for a particular OCM catalyst, the Arrhenius pre-exponential factors and activation energies are adjusted to fit the experimental results [8,9]. Once established, these kinetic mechanisms are utilized in reactor-design optimization algorithms to determine an upper bound. A more comprehensive approach has been taken by Feinberg and co-workers [10,11], who have presented methods for maximizing production rate considering all possible reactor designs. In both cases, optimization is performed with fixed chemical kinetics, and the performance is constrained by the quality of the catalyst used in developing the mechanism. The unintentional result is the de-emphasis of the catalyst's role in obtaining high yields. This is greatly at odds with conclusions arrived at by experimentalists, who have often linked performance to the relative rates of surface reactions.

An early attempt at determining a bound on OCM yield was performed by Labinger [12]. In his paper, Labinger solves a set of ordinary differential equations (ODE) derived via a pseudo-elementary reaction mechanism to ultimately chart methane conversion vs C_2 selectivity. In this model, the surface irreversibly reacts with CH_4, CH_3, C_2H_6, C_2H_4, and $C_3{}^+$ species. Initial rate parameter estimates for his mechanism are derived from experimental data for a mixed Mn–Mg oxide catalyst [13]. By manipulating select rate constants to advantageous values consistent with other experimental catalytic data, Labinger sets an upper bound of 30% yield at 1 atm methane partial pressure for the case where methane and oxygen are reacted separately with the catalyst.

Recently, several issues have been brought to light that warrant re-examining Labinger's upper bound. First, because both heterogeneous and homogeneous steps are necessary for C_2 formation, mass transfer is believed to play a potentially significant role in the OCM yields obtained. Couwenberg et al. [14] identified irreducible mass-transfer limitations on surface-generated reactive intermediates such as methyl radical, whose lifetimes are short compared with the transport time scale. The resulting concentration gradients facilitate second-order processes such as methyl radical coupling to form C_2 species, increasing the yield. It is not possible to capture this effect with an ODE (CSTR or PFR) model; a 2D or 3D simulation is necessary.

Second, at the high temperatures needed for OCM, O_2(g) will be present above the regenerable metal oxide catalyst. This being the case, an industrial OCM process will probably co-feed methane and oxygen to avoid reduction of the catalyst. The presence of O_2(g) introduces many additional complications as it will also quickly undergo reaction with gas-phase radicals, significantly affecting the selectivity and yield. Here, we establish the yield limit for a co-fed CH_4/O_2 system rather than the two-stage system studied by Labinger.

The intricate balance between the need for gaseous oxygen in catalyst activation and its detrimental role in gas-phase oxidation contradicts the notion of simply treating the catalyst as a methyl radical generator. A number of additional interactions occurring between the gas phase and the catalyst surface deserve further attention because of the intimate coupling of heterogeneous and homogeneous reactions. Beyond its role in methyl radical generation, research has also indicated that the catalyst serves as a radical quencher. This removal of detrimental/beneficial gas-phase species can significantly alter the conversion/selectivity trajectory.

Finally, although OCM has long been thought to occur via a catalytic cycle, catalyst researchers have largely focused on only one step in this cycle: reducing the activation energy for hydrogen abstraction from methane. However, for very active catalysts, alternative bottlenecks could be present. For instance, acceleration of hydrogen abstraction typically requires increasing the stability of the resulting surface hydroxyl species. If pushed to extremes, these surface hydroxyls could effectively act as poisons. Understanding the limited combinations of surface energetics that allow for optimum throughput in the catalytic cycle could provide catalyst developers with both a clear target and a tool for screening catalysts.

In this paper, we present a different paradigm for modeling heterogeneous catalysis. Since our goal is to determine whether a fundamental upper bound on OCM yield exists, instead of fixing surface chemistry parameters to match one particular catalyst, we have computed the OCM yield of a range of conceivable catalysts. OCM is a model case study for this approach in that, despite the large number of catalysts examined, a fairly unified surface mechanism has been set forth. The key catalytic cycle consists of a small number of elementary reactions, minimizing the dimensionality of the search space. In each case, beneficial surface reaction rates are set at the upper limit of what is physically achievable. While large uncertainties exist in any one set of experimentally derived kinetic parameters, some of the limits of catalyst behavior are well-known (e.g., the energetics of oxygen adsorption/desorption on metal oxides and diffusion limits on reaction rates). Surface thermochemistry immediately provides a bound on kinetics. Thanks to improvements in computational speed, the use of detailed multicomponent transport models coupled with elementary surface reaction mechanisms is now practical. As shown below, even if one could synthesize a catalyst where all desired reaction rates were maximized and all surface species had optimal thermochemistry, OCM yield would still be significantly restricted by fundamental thermodynamic and transport limitations.

2. Reaction mechanism

Gas-phase rate constants and thermodynamic property data were taken from a library of reactions compiled previously by Mims et al. [15]. This homogeneous model contains almost 450 reversible elementary chemical reactions

Table 1
Proposed surface mechanism for OCM

Reaction		A_f [a]	E_f (kJ/mol)	A_r	E_r (kJ/mol)
$O_2 + 2V^* \leftrightarrow O^* + O^*$	(1)	1.63×10^{22}	0.0	2.39×10^{19}	250
$CH_4 + O^* \leftrightarrow CH_3^{\cdot} + OH^*$	(2)	1.85×10^{13}	94.41	1.91×10^{13}	0.0
$OH^* + OH^* \leftrightarrow H_2O + O^* + V^*$	(3)	2.25×10^{19}	0.0	2.17×10^{22}	94.41
$C_2H_6 + O^* \leftrightarrow C_2H_5^{\cdot} + OH^*$	(4)	1.35×10^{13}	103.80	1.37×10^{13}	0.0
$C_2H_4 + O^* \leftrightarrow C_2H_3^{\cdot} + OH^*$	(5)	1.40×10^{13}	144.71	1.42×10^{13}	0.0
$CH_2O + O^* \leftrightarrow CHO^{\cdot} + OH^*$	(6)	1.35×10^{13}	61.74	1.37×10^{13}	0.0
$CH_3OH + O^* \leftrightarrow CH_3O^{\cdot} + OH^*$	(7)	1.31×10^{13}	108.00	1.33×10^{13}	0.0
$HOO^{\cdot} + O^* \leftrightarrow O_2 + OH^*$	(8)	1.29×10^{13}	0.0	1.31×10^{13}	138.78
$HOO^{\cdot} + V^* \leftrightarrow HO^{\cdot} + O^*$	(9)	1.29×10^{13}	0.0	1.80×10^{13}	110.51
$CH_3OO^{\cdot} + 2V^* \leftrightarrow O^* + OCH_3{}^*$	(10)	1.34×10^{22}	0.0	1.72×10^{19}	386.76
$CH_3OO^{\cdot} + V^* \leftrightarrow O^* + CH_3O^{\cdot}$	(11)	1.08×10^{13}	0.0	1.33×10^{13}	144.49
$CH_3^{\cdot} + O^* \leftrightarrow CH_3O^*$	(12)	1.91×10^{8}	0.0	2.24×10^{13}	233.28
$CH_3O^* + X^{\cdot} \leftrightarrow XH + CH_2O + V^*$	(13)	[b]			
$CH_3O^* + O^* \leftrightarrow OH^* + CH_2O + V^*$	(14)	1.72×10^{19}	0.0	1.69×10^{19}	5.96

A-Factor and E_a values shown are for the case where $\Delta H_{ads} = -250.0$ kJ/mol and $\Delta H_{abs} = 125$ kJ/mol. These are the optimal kinetic parameters for OCM performance as determined by the yield map in Fig. 1.

[a] A-Factors in cm, mol, s units.

[b] A-Factors and E_a values are dependent on the abstracting gas-phase species.

and 115 species. Here, we assume the detailed gas-phase chemistry model is accurate, and focus on the surface kinetics of our hypothetical ideal catalysts. Similar to previous models [9,16], the elementary surface mechanism used is shown in Table 1. Reaction (1) describes the one-step dissociative chemisorption of oxygen. The resulting activated oxygen serves to abstract hydrogen from methane in reaction (2) via an Eley–Rideal mechanism, generating methyl radicals that then couple in the gas phase. To complete this catalytic cycle, two surface hydroxyls combine to form water in reaction (3), regenerating a vacancy site in the process.

In addition to these steps, reactions (4)–(7) describe hydrogen abstraction from the major products. Inclusion of these reactions undoubtedly reduces yields, yet the lower/similar C–H bond energies of ethane, ethene, methanol, and formaldehyde make these species as susceptible to hydrogen abstraction as methane. We assume that, at OCM temperatures, the surface interacts with these species in a manner similar to how it reacts with methane. As a partial proof of their necessity, previous simulations done by Hargreaves, Hutchings, and Joyner found that failure to include reaction (6) resulted in concentrations of formaldehyde that were never experimentally observed [17].

The appropriateness of assuming comparable hydrogen abstraction rates from C–H bonds with similar strengths may come into question given the experimentally observed rate constants for methane versus ethene combustion. Shi, Rosynek, and Lunsford [18], through isotope labeling experiments, have determined that, for several OCM catalysts, the overall rate for ethene combustion is ~ 3–5 times larger than that for methane combustion. This may seem surprising since the C–H bond energy for ethene is greater than that for methane. When considering the overall rates for the combustion of methane and ethene, however, we must consider

the fact that this process involves several elementary reactions. Following hydrogen abstraction, the resulting methyl and vinyl radical species must undergo further reaction to form CO_2. Unlike vinyl radicals, which are known to react very quickly with O_2(g) to form CO_x precursors, methyl radicals are relatively unreactive with O_2 [15]. The initial methyl–O_2 adduct is unstable at OCM temperatures and falls apart back to methyl and O_2(g). Our calculations suggest that all the surface-mediated routes from CH_3 to CO_2 involve an endothermic reaction. Thus, it is not surprising that ethene is converted to CO_x more rapidly than methane, even though the rate of the first step is not very different.

While the main function of the catalyst is to act as a source for radical species, several researchers have discussed the radical quenching abilities of solid surfaces [19,20]. Such quenching reactions may provide a means for the removal of detrimental gas-phase species and thus inhibit negative gas-phase reaction channels. Peroxy species have been shown to facilitate undesirable gas-phase deep oxidation pathways [15,21]. Therefore, we have also included what we consider to be the major surface-mediated peroxy radical quenching reactions (reactions (8)–(11)). These reactions either involve a very fast H abstraction or cleavage of the very weak peroxide bond.

One aspect of the surface mechanism that is not clear is the role of the catalyst in heterogeneous deep oxidation. Many researchers have speculated about such pathways, but a great deal of debate still exists as to the appropriate treatment of such pathways [22]. Deep oxidation products are often blamed on the presence of unselective, surface-adsorbed oxygen species that have not had time to be incorporated into the oxide lattice [16]. In addition, unwanted secondary reactions of ethene, such as reaction of the ethene double bond with the surface, also eventually lead to deep oxidation products. Both of these heterogeneous reaction pathways result in lower C_2 yields. Since our ultimate goal is to obtain an upper bound on the OCM yield, we have limited the heterogeneous contribution to deep oxidation only to indirect pathways. Perhaps the most critical examples of indirect deep oxidation involve secondary reactions of ethane and ethene. Surface-mediated hydrogen abstraction from these species result in radicals that then degrade via gas-phase channels to CO_x species. Even under ideal circumstances, they are likely unavoidable and play a large role in limiting OCM yields. Thus, they have been included in the surface mechanism in the form of reactions (4) and (5).

Indirect, surface-mediated deep oxidation pathways were also considered in the treatment of surface methoxy species. From an energetic standpoint, we expect that the collision of methyl radicals with the catalyst favors methoxy formation (reaction (12)). Such intermediate species have been observed in related, lower temperature reactions involving methanol and methane. In situ DRIFT studies of OCM over lanthana catalysts, however, detected only trace amounts of these species under reaction conditions [22]. Thus, we hypothesize that surface methoxy species are unstable at high temperature, either dissociating or being quickly subjected to further degradation. Examination of methoxy degradation routes in lower temperature partial oxidation reactions provides some clues. In situ DRIFT studies by Li et al. [23] on the decomposition and adsorption products of methanol and formaldehyde on CeO_2 found that methoxy species degrade in the following sequence of reactions:

$$CH_3O \rightarrow HCOO \rightarrow CO_2 \text{ (adsorbed carbonate)}.$$

Surface formaldehyde is an intermediate in this process. In certain cases, this sequence appears to terminate before carbonate formation. Selective partial oxidation catalysts such as MoO_3/SiO_2 have been found to convert methane to formaldehyde with high selectivity without any evidence of surface carbonate [24]. Yang and Lunsford theorized that the rate of formaldehyde desorption from the surface was rapid enough to prevent formaldehyde degradation [24]. Perhaps this is one reason why MoO_3 species have been found to have superior performance in partial oxidation reactions. Under ideal circumstances, we assume that surface methoxy species are converted to formaldehyde through reactions (13) and (14). Upon formation, however, formaldehyde is quickly desorbed from the surface.

Having developed an a priori surface mechanism, both Arrhenius pre-exponential factors and activation energies were needed to specify the forward and reverse rate constants. To set an upper bound on catalyst activity, no additional barriers to reaction were considered beyond those required by thermochemistry. Thus, in the case of endothermic reactions, the activation energy was set equal to the enthalpy of reaction, while exothermic steps were assumed to have no barriers.

For steps involving gas molecules striking the surface, upper bounds on the Arrhenius pre-exponential factors were calculated using collision theory. Pre-exponential factors for reactions involving only surface species were determined using simplified transition-state arguments [25]. To set an upper bound on catalyst turnover, sticking coefficients were initially set to unity. The only exception to this was the reaction of methyl radicals with the catalyst surface. Tong and Lunsford [26] have presented evidence suggesting that the sticking coefficient for methyl radicals on good OCM catalysts is significantly less than unity, approximately 10^{-7}. As shown later, an ideal OCM catalyst would certainly not have a collision-controlled rate for this detrimental reaction.

Given the number of surface reactions, this approach appears to result in a dauntingly large multidimensional search space. We will show, however, through a variety of arguments, that the number of truly independent reaction enthalpies is relatively small. A brief description of the methodology is given below. For additional details please refer to Appendix A. The enthalpy associated with reaction (1) was the first of two independently specified reaction enthalpies. A range of oxygen adsorption enthalpy values spanning -75 to -300 kJ/mol was examined, which includes literature values obtained for oxygen adsorption on

a wide variety of metal oxides [27]. Enthalpies for this reaction were examined at fixed intervals of 25 kJ/mol. Similarly, the enthalpy for reaction (2), the hydrogen abstraction reaction of methane, was independently fixed at 25 kJ/mol increments in the range of 75 to 200 kJ/mol. This broad range centers around the average hydrogen abstraction energy for Li/MgO [28] and Li/Sn/MgO [9], two of the most active and well-characterized OCM catalysts to date. When the values of reactions (1) and (2) are independently set, the reaction enthalpy associated with reaction (3) is automatically fixed according to the thermochemistry of the overall catalytic transformation of methane and oxygen to methyl radicals and water.

Upon specification of the enthalpy of methane hydrogen abstraction, the remaining barriers for ethane, ethene, formaldehyde, and methanol were scaled according to the difference in C–H bond energy of these species relative to methane. To distinguish the bond energies of MO–H versus MO–CH_3, the differences in bond strength for several hydrocarbon species of the type RO–H and RO–CH_3 were compared [29]. Finally, surface formaldehyde was assumed to desorb from the surface with no barrier.

Altogether, there are five surface species whose thermochemistry is unknown. One of these is fixed by the requirements of thermodynamic consistency, one is set relative to the energy of OH^* by analogy, one is set by defining the zero of energy, and two are allowed to float within a physically reasonable range. To fully span the two-dimensional subspace of surface energetics requires a total of 60 independent calculations.

3. Model formulation

As a first approximation of flow through a packed bed, the bed was visualized as a series of parallel, noninteracting, isothermal cylinders. These cylinders were considered lined with our hypothetical catalyst, and intraparticle microporosity was ignored. To maximize catalyst site density, a cubic crystal structure was examined, where all exposed surface oxygen atoms were assumed to be potentially active sites for OCM. The resulting site density was calculated to be $\sim 1 \times 10^{-9}$ mol/cm^2. Site densities from other crystal structures are comparable.

To maximize methyl radical production, the smallest allowable pipe diameter was selected to increase the surface-to-volume ratio of the pipe and hence the heterogeneous phase contribution. The cylinder diameter (0.02 cm) was determined by averaging the resulting void space of meshed particles (20–60) typically employed in OCM tests. As with most laboratory-scale OCM experiments, simulations were performed at 1 atm. The flow velocity was fixed at 5.25 cm/s. Higher velocities were avoided as they are observed to result in significant pressure drops during packed-bed studies. Cylinder length was not fixed, but adjusted to maximize the yield for each hypothetical catalyst and reaction condition.

Using the various surface kinetic models described earlier, the typical range of packed-bed conditions was simulated to find a maximum yield. Specifically, temperatures ranging from 700 to 800 °C were examined, with methane to oxygen molar feed ratios of 2:1 to 10:1. Similar to experimental catalyst screening conditions, a dilute feed stream of 15% reactants was employed. The series of equations describing multicomponent transport and chemical reaction occurring throughout the catalyst-lined cylinder was solved using the commercial modeling package, CRESLAF [30]. This solves the conservation equations for momentum, species, and energy in a two-dimensional channel, assuming laminar flow, neglecting axial diffusion, and utilizing the ideal gas law as the equation of state. A more detailed discussion of the formulation can be found in either the CRESLAF manual [30] or in the publications of Coltrin et al. [31,32]. Concentration profiles output from CRESLAF simulations were used in calculating methane conversion and C_2 selectivities down the catalyst bed. Yields versus axial position were then calculated, and the maximum yield was selected in forming yield maps. As mentioned earlier, CRESLAF was utilized to capture the potentially significant effects of radial gradients in radical concentration. For comparison, calculations were also made with a plug flow approximation using PLUG [30].

4. Results and discussion

4.1. Yield bounds of nonporous catalysts

Maximum yields of the aforementioned subspace of surface energies were tabulated in yield maps such as Fig. 1. Results displayed are for reactor conditions of $T = 800$ °C and CH_4:O_2 = 2:1, as these conditions were found to result in the highest yields. Even under the most optimal set of surface energies, however, the maximum yield only approaches 14%. In contrast, yields cited for superior OCM catalysts exceed 20%.

Several possible explanations exist for this discrepancy. One possibility is that the elementary mechanism does not accurately represent the surface kinetics of high-yield OCM catalysts. An alternative mechanism, such as one that differentiates between oxygen species, may be more appropriate. Assuming the kinetic mechanism employed is correct, however, another potential pitfall is the inadvertent maximization of a negative reaction channel. We do not believe this is the case. With respect to the main catalytic cycle, our belief is that high OCM yields are attained via rapid catalytic turnover. The generation of a high methyl radical concentration should promote coupling to C_2 species over deep oxidation. This is due to the second-order nature of the coupling reaction. One area where the reduction of activation energies to enthalpic values was presumably

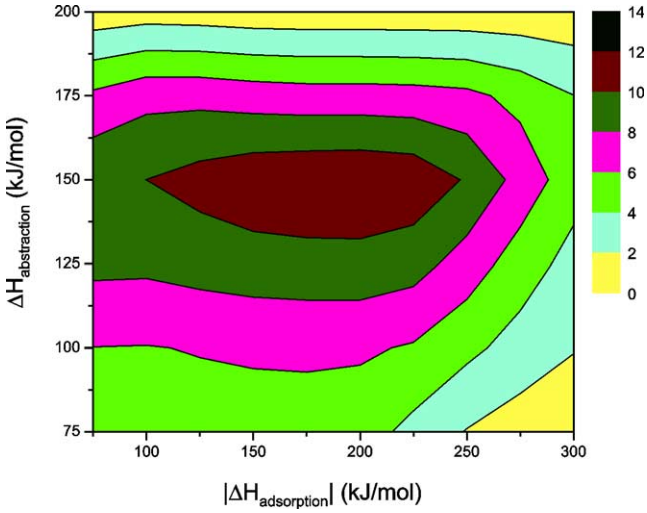

Fig. 1. OCM yield bound map for a nonporous catalyst as determined by an axisymmetric, multicomponent reacting flow simulation. Each grid point represents a single simulation performed using a specific set of surface reaction parameter values. The various parameter sets employed are generated through independent selection of O_2 dissociative adsorption enthalpy (reaction (1)) and CH_4 hydrogen abstraction enthalpy (reaction (2)) in the main OCM catalytic cycle. Details are given in Section 2. $T = 800\,^{\circ}\mathrm{C}$, $P = 1$ atm, CH_4:O_2:N_2 feed ratio = 2:1:17.

sub-optimal was in reaction (14), the conversion of surface methoxy species to formaldehyde. Concern regarding the overexpression of this reaction prompted examining the effects of removing this reaction pathway. The resulting impact on C_2 yield, however, was found to be minor. While rate-of-production analysis shows reaction (14) to be the primary surface channel for the formation of formaldehyde, its impact is ameliorated by the low formation rate of surface methoxy species. Finally, the influence of various radical-quenching reactions was also evaluated. As shown later, manipulations of the sticking coefficients for these reactions indicate that the optimal kinetic parameters were used.

The source of the yield discrepancy can likely be attributed to some oversimplification, whether physical or kinetic, of the real packed bed. For example, nonhomogeneity in temperature as well as in catalyst surface undoubtedly has a significant impact on the resulting yield trajectory. One important cause of the lower-than-expected yields is the geometric constraint imposed on the model. By modeling the system as a series of catalyst-lined pipes, the bulk of catalyst sites provided by porosity is neglected. As a first attempt to take into account this phenomenon, transport effects within the pores themselves were ignored and the surface site densities were simply increased. Barring the possibility of selective transport such as oxygen sieving, it is believed that this should provide an upper bound on what really occurs in porous catalysts.

4.2. Model for microporous packed-bed catalysts

To approximate the extent to which microporous networks could contribute to catalyst active sites, we employed a geometric argument based on a sphere-packing model of catalyst particles [33,34]. The sieved particles constituting the packed bed were assumed to consist of agglomerated networks of nonporous microspheres. Assuming microspheres of a given uniform size, the number of microspheres making up the sieved particle can be calculated. From this, the total surface area of the sieved particles is determined.

As expected, reducing the microsphere size results in increased total surface area. Constraints exist, however, as to the area that may be effectively utilized for OCM. The effective surface area cannot be simply increased by selecting smaller and smaller microspheres. Reyes and Iglesia [34] have shown that, for a uniform agglomerate of microspheres, the average pore radius is roughly half that of the microsphere radius. This average pore diameter must exceed the methyl radical mean free path to allow significant methyl radical coupling in the gas phase to form the C_2 products. Under the reaction conditions studied, the mean free path is approximately 200 nm. In addition, coupled products such as ethene, once formed, must diffuse out of the particle without further reaction with the surface (otherwise, they will be converted to CO_x products). To determine the particle shell thickness wherein OCM can take place without destruction of the ethene produced, we employ a random walk argument. The mean time for a randomly formed ethene molecule to contact the pore wall is approximated by $(2r_p)^2/12D$ where r_p is the average pore radius and D is the diffusion coefficient of ethene. This time is then scaled via the inverse of the reaction probability of ethene with the surface. This estimates the average time elapsed prior to further ethene reaction. Using this value of time, the mean square distance that ethene molecules can travel in the pores before being consumed can be calculated. Thus, an estimate of the thickness of the particle shell that can be utilized effectively for OCM may be obtained. Fig. 2 shows the ratio of the accessible surface area to the geometric surface area of the pipe. As expected, since the time before wall reaction increases with the square of the pore diameter, ethene can safely diffuse out of particles made of large microspheres. However, the size of the microspheres then limits the gain in surface area. The effectiveness of particles composed of small microspheres is strongly influenced by the reaction probabilities of the molecules being examined. With large reaction probabilities, the accessible number of sites inside the particles is much smaller than that derived from the microsphere's external surface area. With a barrier of 100 kJ/mol for ethene surface abstraction at 800 °C, the reaction probability of ethene is $\sim 1.4 \times 10^{-5}$ per collision with the surface. This results in a maximum effective surface area that is 2 orders of magnitude larger than the geometric surface area used in computing Fig. 1.

4.3. Yield bounds for microporous OCM catalysts

To simulate the contribution of this additional surface area, the original site density was increased by 2 orders

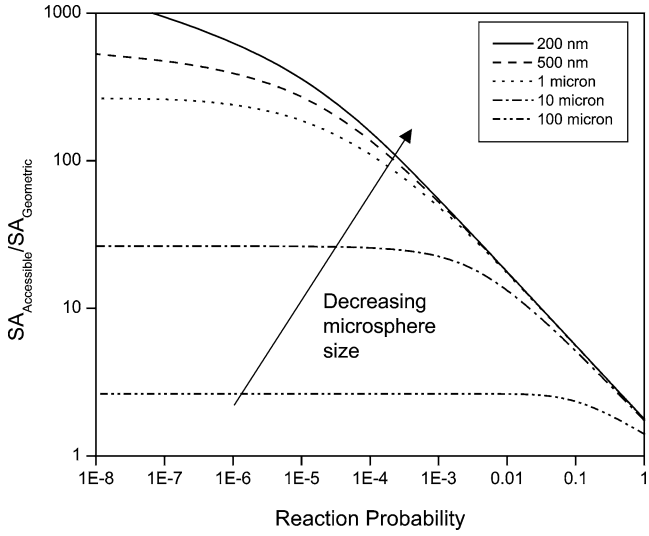

Fig. 2. Impact of microsphere size on accessible pore surface area of sieved particles. Smaller particles show significant enhancement of accessible surface area with decreasing ethene reaction probability. In our model, the reaction probability $\sim 10^{-5}$, so microporosity can increase the effective surface area by 2 orders of magnitude. Bed void fraction $= 0.2$, particle porosity $= 0.3$.

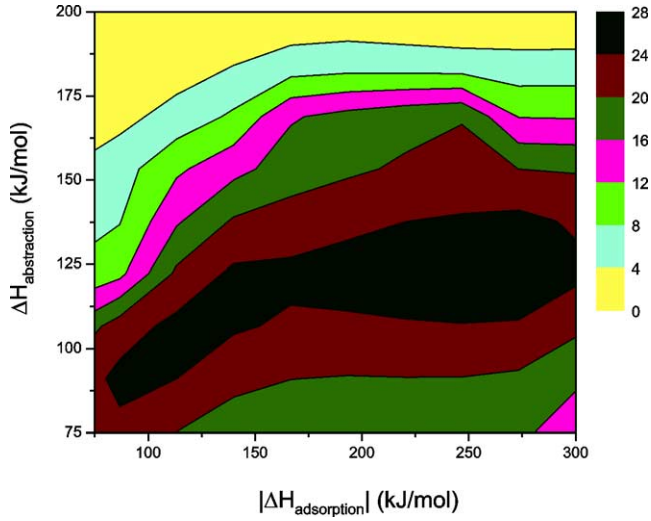

Fig. 3. OCM yield bound map with 100× the effective site density used in Fig. 1 (modeling the increased surface area due to microporosity). Other parameters used are identical to those employed in generating Fig. 1. Note the strong effect of surface area on the yield bound.

of magnitude such that the total number of active sites was conserved. As shown in Fig. 3, overall OCM yields of up to 28% may be obtained. While modification of the site density to capture internal micropore contributions is a rough approximation, it is interesting that the consequent upper bound is comparable to yields reported for the best experimental OCM catalysts.

One important result from Fig. 3 is that superior yields are observed only within a narrow window of catalyst thermochemistry. This contradicts earlier predictions that the catalyst plays a minor role in determining OCM performance [8,35]. While the unavoidable secondary reactions of ethane and ethene undeniably shape the maximum yields attainable, Fig. 3 testifies to the uniqueness of each catalyst in determining that ultimate bound. The fact that maximized yields occur under conditions where the methane hydrogen abstraction energy is not minimized raises an important possibility. While two of the three critical reactions in the main catalytic cycle can be independently fixed, the energetics of the third reaction is constrained by thermodynamics. This interconnectedness complicates the notion of rational catalyst design. For instance, the ease with which a material adsorbs oxygen has a profound effect on how easily water can be desorbed. Targeting efforts exclusively to improve a single catalyst feature (e.g., hydrogen abstraction) may simply result in bottlenecks from the other surface reactions.

4.4. Reaction pathway analysis

To test this hypothesis, the main catalytic cycle was analyzed via Campbell's degree of rate control [36]. $X_{\mathrm{RC},i}$, the degree of rate control for step i, is defined as:

$$X_{\mathrm{RC},i} = \frac{k_i}{r}\left(\frac{\delta r}{\delta k_i}\right)_{K_{\mathrm{eq},i},k_j},$$

where r is the overall rate of the catalytic cycle, k_i and $K_{\mathrm{eq},i}$ are the forward rate constant and equilibrium constant for step i, respectively, and k_j's are the rate constants for the remaining steps. Implementation of this method was done numerically. MATLAB was used to solve the steady-state rate equations in the main catalytic cycle for site fraction values. The site fractions obtained from this simplified model corresponded quite well to values obtained via PLUG and CRESLAF calculations at a fraction of the computation cost. The influence of each step on the overall rate was then determined by increasing the values for both k_i and k_{-i} by a small factor and recalculating the steady-state rate. This was repeated using smaller incremental increases until the true differential limit was approached.

Fig. 4 shows the resulting X_{RC} values for the methane hydrogen abstraction (reaction (2)) of the main catalytic cycle. In almost all cases, hydrogen abstraction was found to be rate-limiting. At low $\Delta H_{\mathrm{abstraction}}$, however, increases in $|\Delta H_{\mathrm{adsorption}}|$ result in the appearance of an alternative rate-limiting step. This effect, however, is only important at the fringe of catalyst energetics studied and does not explain why the computed OCM yield drops off in the range of $\Delta H_{\mathrm{abstraction}} < 125$ kJ/mol and $-100 > \Delta H_{\mathrm{adsorption}} > -250$ kJ/mol. In fact, hydrogen abstraction remains the rate-determining surface reaction throughout this region, which would seem to imply that further reductions in the hydrogen abstraction barrier would result in even greater methyl radical production. This is indeed the case. At $\Delta H_{\mathrm{adsorption}} = -200$ kJ/mol, as $\Delta H_{\mathrm{abstraction}}$ is decreased from 125 to 75 kJ/mol, an approximate 2 orders of magnitude increase

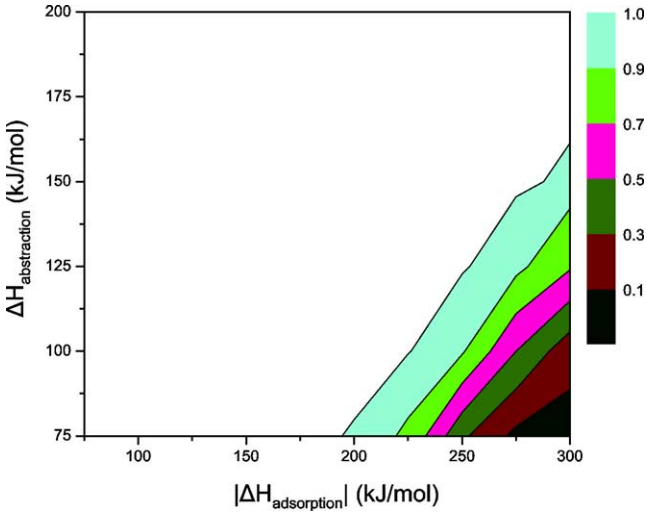

Fig. 4. Contour map of potential rate-limiting behavior by surface methane hydrogen abstraction (reaction (2)) using Campbell's degree of rate control method. Reaction (2) is rate-controlling in almost all cases.

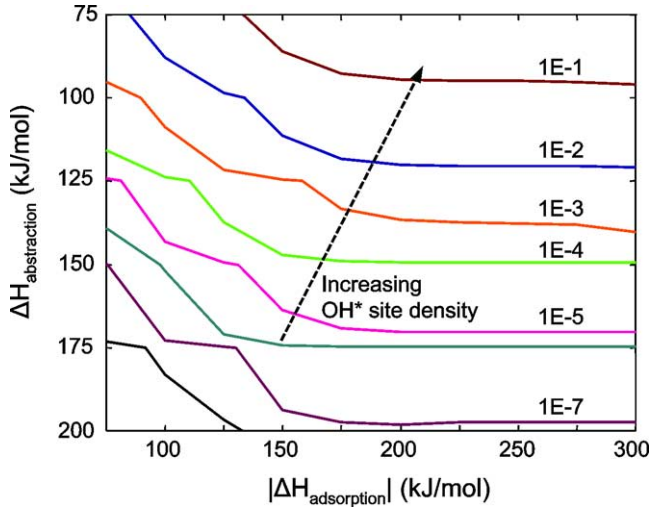

Fig. 5. Variation in steady-state OH* site fraction at point of peak methyl radical production with changes in catalyst chemistry ($\Delta H_{\text{abstraction}}$, $\Delta H_{\text{adsorption}}$).

in the methyl radical formation rate are observed. Overall C_2 yields, however, drop from 26.4 to 17.6%. The contradiction between high methyl radical production and low overall OCM yield hints at the onset of a new channel that competes with gas-phase methyl radical coupling. To quantify the consumption channels for methyl radicals, small sections of the catalyst-lined pipes were analyzed using Chemkin's AURORA CSTR model. This allowed for the convenient extraction of reaction sensitivity and production rate values. To mimic the 2D model system, catalyst surface area-to-volume ratios were maintained. A cross section of abstraction enthalpies was studied at $\Delta H_{\text{adsorption}} = -200$ kJ/mol using gas and surface mole fraction inputs obtained from earlier CRESLAF simulations. Small residence times ($\tau = 10^{-2}$ and 10^{-3} s) were selected for CSTR simulations to take snapshots of behavior at different points along the catalyst-lined pipe. Since the axial length scale for reaction changes with $\Delta H_{\text{abstraction}}$ (reactants are converted to products in a much shorter distance at low $\Delta H_{\text{abstraction}}$), changes in production/consumption channels were compared at z values of identical conversion.

At 20% conversion, when $\Delta H_{\text{abstraction}} = 150$ kJ/mol, methyl radical consumption is dominated by gas-phase coupling to form ethane. This reaction channel accounts for $\sim 55\%$ of methyl radical consumption. Several additional gas-phase consumption channels are also present, such as $C_2H_6 + CH_3 \rightarrow C_2H_5 + CH_4$ and $CH_3 + O_2 \rightarrow CH_3OO$, which account for ~ 10 and $\sim 9\%$ of CH_3 consumption. Under these conditions, the surface reaction, $OH^* + CH_3 \rightarrow CH_4 + O^*$, accounts for only 12.6% of methyl radicals consumed. As $\Delta H_{\text{abstraction}}$ is reduced, however, this surface reaction becomes increasingly important. At $\Delta H_{\text{abstraction}} = 125$ kJ/mol, $OH^* + CH_3 \rightarrow CH_4 + O^*$ consumes $\sim 48\%$ of the methyl radicals produced, increasing further to 92.6 and 99.2% at $\Delta H_{\text{abstraction}} = 100$ and 75 kJ/mol, respectively. In some cases, this reverse reaction is accelerated to a degree such that reaction (2) becomes quasi-equilibrated. For $\Delta H_{\text{abstraction}} < 125$ kJ/mol and larger $|\Delta H_{\text{adsorption}}|$ values, an analysis of the reversibility of reaction (2) reveals values approaching 1 [37]. The appearance of this surface reaction as a significant competitive channel for CH_3 consumption is not due to a change in its activation energy, which remains fixed in our model at 0 kJ/mol. Instead, as Fig. 5 shows, the steady-state population of OH* rises dramatically as $\Delta H_{\text{abstraction}}$ is decreased, increasing from $\theta_{OH^*} < 10^{-8}$ at $\Delta H_{\text{abstraction}} = 200$ kJ/mol to $\theta_{OH^*} \sim 0.3$ at $\Delta H_{\text{abstraction}} = 75$ kJ/mol. Due to the interconnected nature of surface reaction steps, as $\Delta H_{\text{abstraction}}$ is decreased and $|\Delta H_{\text{adsorption}}|$ increased, hydroxyl removal becomes increasingly endothermic. The outcome is a dramatic increase in the steady-state equilibrium concentration of OH* species on the surface, which results in the reaction $OH^* + CH_3 \rightarrow CH_4 + O^*$ dominating over the desired methyl radical coupling.

While the increasing role of the surface back-reaction $OH^* + CH_3 \rightarrow CH_4 + O^*$ reduces the benefit of going to lower values of $\Delta H_{\text{abstraction}}$, it still cannot explain the drop-off in the computed OCM yield. At a conversion of 20% and $\Delta H_{\text{adsorption}} = -200$ kJ/mol, decreasing $\Delta H_{\text{abstraction}}$ from 125 to 100 kJ/mol results in an order-of-magnitude increase in methyl radical production. While a larger portion of these methyl radicals are reacted back to CH_4 (92.6 versus 47.5% for $\Delta H_{\text{abstraction}} = 125$ kJ/mol), the steady-state concentration of CH_3 is still ~ 2 times higher. Thus, methyl radical coupling is always enhanced at lower values of $\Delta H_{\text{abstraction}}$. The decrease in yield that is observed at $\Delta H_{\text{abstraction}} < 125$ kJ/mol can only be explained if we examine the concurrent changes occurring in the other surface reactions. As $\Delta H_{\text{abstraction}}$ for methane is reduced, an identical barrier reduction occurs in the remaining hydrogen abstraction steps. In particular, the reactions of O* with the C_2 products (C_2H_6 and C_2H_4) are also accelerated by

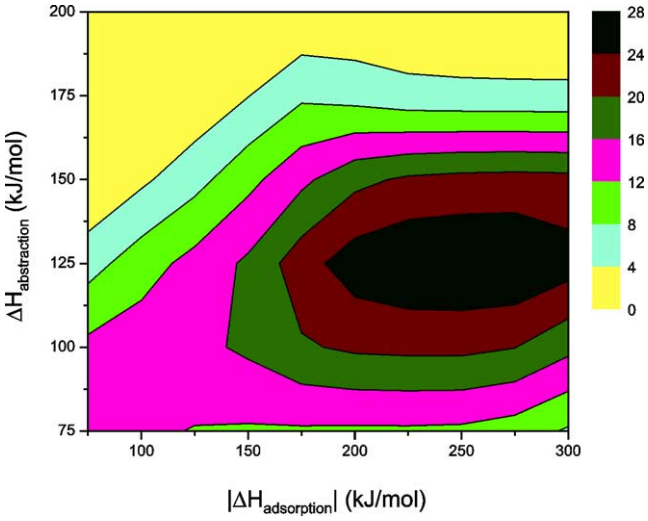

Fig. 6. OCM yield bound map as determined via plug flow simulation. The various parameter sets employed as well as modeling conditions are identical to those used in generating Fig. 3. For high surface-to-volume ratios, the plug flow approximation is accurate over most of the range. $T = 800\,^{\circ}\mathrm{C}$, $P = 1$ atm, CH_4:O_2:N_2 feed ratio = 2:1:17.

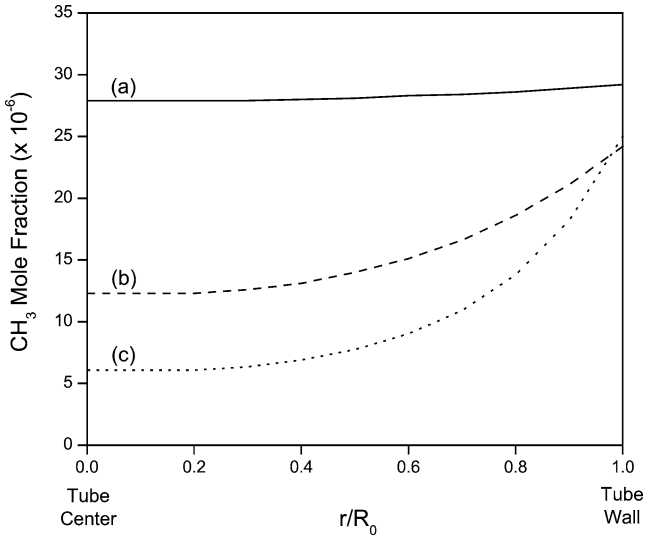

Fig. 7. Methyl radical mole fraction versus fractional radial distance at $z = 0.2$ cm for $r =$ (a) 0.01 cm, (b) 0.05 cm, and (c) 0.1 cm. For larger radii, the methyl radical concentration is significantly higher near the catalyst surface than in the middle of the channel, and the plug flow approximation is not accurate.

an order of magnitude. But unlike hydrogen abstraction of CH_4, once these C_2 species undergo hydrogen abstraction to form their radical counterparts, they are quickly reacted away. In the case of C_2H_5, many of these gas-phase consumption reactions simply lead to ethylene formation (i.e., $C_2H_5 \rightarrow C_2H_4 + H$ and $C_2H_5 + O_2 \rightarrow C_2H_4 + HO_2$). However, C_2H_3 formed from C_2H_4 is rapidly consumed by O_2 in the reactions, $C_2H_3 + O_2 \rightarrow HCO + CH_2O$ and $C_2H_3 + O_2 \rightarrow C_2H_3O^{\cdot} + O$. At $\Delta H_{\text{abstraction}} = 125$ kJ/mol, these reactions destroy 96% of the C_2H_3 formed; the products ultimately become unwanted CO_x. Importantly, these negative gas-phase consumption channels remain dominant at low $\Delta H_{\text{abstraction}}$. While the back-reaction $OH^* + CH_3 \rightarrow CH_4 + O^*$ competes effectively with methyl coupling (which is slow because it is second order in the radical concentration), the comparable back-reaction $C_2H_3 + OH^* \rightarrow C_2H_4 + O^*$ is not as competitive with the very fast $C_2H_3 + O_2$ reaction. For $\Delta H_{\text{abstraction}} > 100$ kJ/mol, $< 4\%$ of the C_2H_3 formed is consumed by surface reactions. The increased rate of C_2 destruction continues largely uninhibited by surface back-reactions as $\Delta H_{\text{abstraction}}$ is lowered, and eventually outstrips the corresponding increases in C_2 formation with the more active catalyst.

4.5. *Plug flow approximation vs 2D simulation*

To quantify the magnitude of potential yield improvements due to irreducible mass-transfer limitations [9,14] on methyl radicals, an identical yield map was created using the plug flow approximation (Fig. 6). For most values of the surface thermochemistry, the plug flow yield closely approximates the multidimensional simulation. The combination of $\Delta H_{\text{abstraction}} = 125$ kJ/mol and $\Delta H_{\text{adsorption}} = -250$ kJ/mol was selected to further examine the role or lack thereof of CH_3 mass transfer on OCM yield. Fig. 7 shows the methyl radical profile for the original tube radius of 0.01 cm as well as those for increased radii of 0.05 and 0.1 cm at $z = 0.2$ cm. No significant gradient of methyl radicals was observed for the original radius. A rate-of-production analysis comparing methyl radical coupling near the wall as opposed to the channel center reveals only minor differences: $\sim 4\%$ difference at $z = 0.2$ cm. A simple Damkohler reaction-diffusion analysis gives the expected length scale of the methyl radical gradient to be ~ 0.02 cm. At $r = 0.01$ cm, the walls of the tube remain within the gradient layer, resulting in overlap with the gradient from the opposing wall. It is only when the tube radius is increased that significant CH_3 gradients are seen. When this occurs, the beneficial impacts due to irreversible mass transport limitations can be large. Due to the second-order nature of methyl radical coupling, the higher concentration of methyl radicals near the catalyst surface results in an increased rate of methyl radical coupling and overall C_2 yield. When comparing the maximum yields for various diameters, however, we have found the yield predicted by the multidimensional model to be lower for larger diameter cases. Thus, while irreducible mass transport effects can significantly increase yields under certain conditions, this benefit is diminished by the fact that such effects are largest at suboptimal operating conditions. To maximize yields, very high surface-to-volume ratios are required, so the spatial dimensions become small enough that diffusion across the channels becomes competitive with radical reactions. Under this condition, the irreducible mass transfer limitation vanishes and plug flow approximations are fairly accurate.

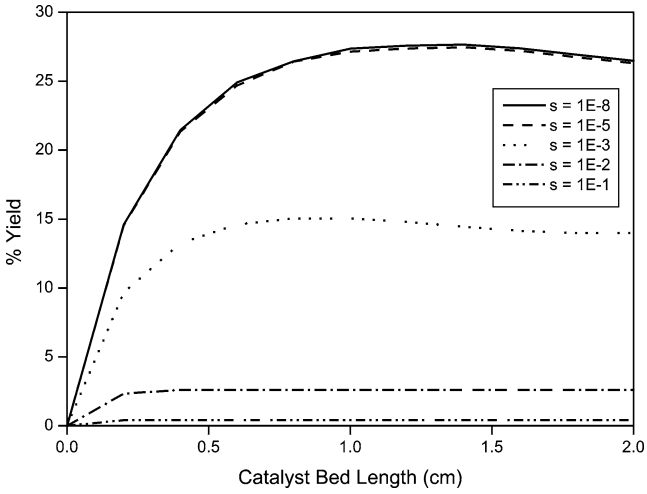

Fig. 8. Influence of CH_3 quenching reaction sticking coefficient on OCM C_2 yield bound. Modeling conditions: $\Delta H_{\text{abstraction}} = 125$ kJ/mol, $|\Delta H_{\text{adsorption}}| = 250$ kJ/mol, $T = 800\,^{\circ}\text{C}$, $P = 1$ atm, CH_4:O_2:N_2 feed ratio = 2:1:17. Low CH_3 sticking coefficients similar to those measured experimentally [27] appear to be necessary for effective OCM catalysts.

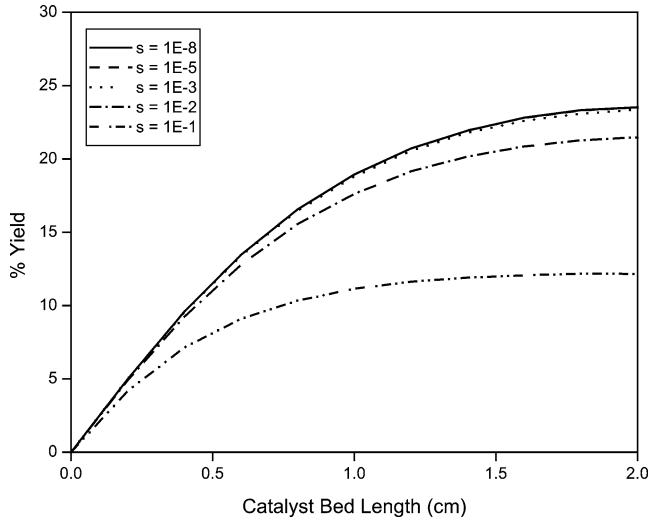

Fig. 9. Influence of CH_3 quenching reaction sticking coefficient on OCM C_2 yield bound at alternative surface conditions: $\Delta H_{\text{abstraction}} = 100$ kJ/mol, $|\Delta H_{\text{adsorption}}| = 75$ kJ/mol, $T = 800\,^{\circ}\text{C}$, $P = 1$ atm, CH_4:O_2:N_2 feed ratio = 2:1:17. Under these conditions, the yield bound is less sensitive to the sticking coefficient value than under the conditions of Fig. 8.

4.6. Importance of surface radical quenching

As an alternative to coupling, methyl radicals near the surface can also react with the catalyst to form surface methoxy species via reaction (12). Poor OCM performance has been previously blamed on large sticking coefficients for methyl radical quenching [38,39]. As mentioned earlier, experimental work by Lunsford et al. [28] seems to indicate that the sticking coefficient for methyl radicals on good OCM catalysts is significantly less than unity. Moreover, Tong and Lunsford inferred a lower limit on the methyl radical sticking coefficient of 10^{-8} [26]. (One caveat is that these sticking coefficients were determined under conditions different from actual OCM conditions. Also, the physical origin of the low methyl radical uptake rate is not known; in our simulations we have just reduced the A-factor.) Fig. 8 highlights the impact of the methyl radical sticking coefficient on catalyst yield for $\Delta H_{\text{abstraction}} = 125$ kJ/mol and $\Delta H_{\text{adsorption}} = -250$ kJ/mol. The extent to which this negative reaction channel competes with gas-phase methyl radical coupling plays a significant role in determining attainable C_2 yields. While it is difficult to imagine a sticking coefficient of 10^{-8} relative to other surface reactions (unless there is a barrier or the surface species is only weakly bound), we do see significant improvements in selectivity at more moderate values for the methyl radical sticking coefficient. A value of 10^{-5} was used as the sticking coefficient in generating Figs. 1 and 3; Fig. 8 suggests that as long as the sticking coefficient is below 10^{-3}, the yield predictions will be similar.

The sensitivity to reaction (12) depends on the surface thermochemistry. For example, Fig. 9 shows the impact of changing the sticking coefficient for a catalyst with $\Delta H_{\text{abstraction}} = 100$ kJ/mol and $\Delta H_{\text{adsorption}} = -75$ kJ/mol. Unlike results at $\Delta H_{\text{abstraction}} = 125$ kJ/mol and $\Delta H_{\text{adsorption}} = -250$ kJ/mol in Fig. 8, these conditions seem more tolerant of higher sticking coefficients. The robustness of a particular set of surface energies with regard to reaction (12) provides us with an additional criterion to further narrow the window of desirable surface energetics for OCM catalysts. While both sets of surface energetics achieve yields in excess of 25%, the conditions of $\Delta H_{\text{abstraction}} = 100$ kJ/mol and $\Delta H_{\text{adsorption}} = -75$ kJ/mol may be more desirable as they are less subject to the additional requirement of a low methyl radical sticking coefficient.

Although surface reaction of methyl radicals is clearly undesirable, radical quenching was found to be advantageous under some circumstances. Studies manipulating the rate of HO_2 quenching by the catalyst (reactions (8) and (9)) via their sticking coefficients show that the catalyst plays an active role in controlling detrimental HO_2 radical populations. As shown in Fig. 10, while reducing HO_2 quenching increases conversion, the selectivity drops dramatically, leading to an overall decrease in yield. As shown by Mims et al. [15], HO_2 facilitates deep oxidation in the gas phase, primarily through the reaction $HO_2 + CH_3 \rightarrow CH_3O + OH$. Reaction sensitivity and rate-of-production values were extracted with AURORA for surface conditions of $\Delta H_{\text{abstraction}} = 125$ kJ/mol and $\Delta H_{\text{adsorption}} = -250$ kJ/mol, using gas and surface mole fraction inputs at $z = 0.2$ cm obtained from earlier 2D simulations. When the sticking coefficient is set to 1, $> 99\%$ of HO_2 in the system is removed through surface quenching. In contrast, with an HO_2 sticking coefficient of 10^{-5}, an insignificant portion of HO_2 is consumed at the surface. The difference in HO_2 surface quenching reduces the predicted upper bound on C_2 yield from 27 to 21%.

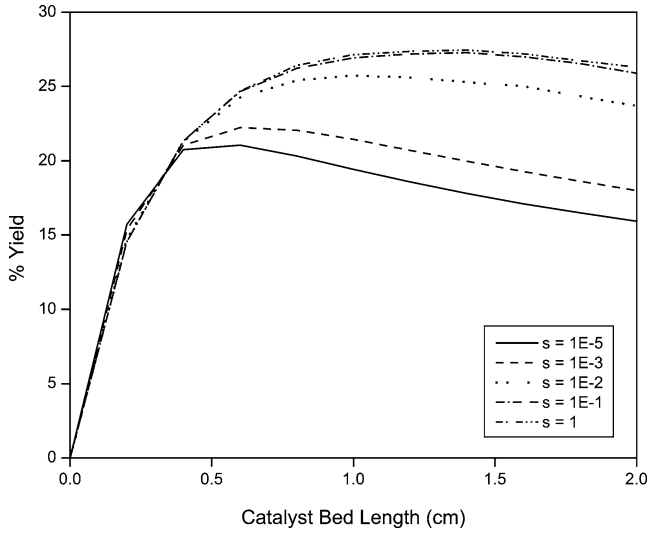

Fig. 10. Impact of HO_2 sticking coefficient on OCM C_2 yield bound. Modeling conditions: $\Delta H_{\text{abstraction}} = 125$ kJ/mol, $|\Delta H_{\text{adsorption}}| = 250$ kJ/mol, $T = 800\,^{\circ}\text{C}$, $P = 1$ atm, CH_4:O_2:N_2 feed ratio = 2:1:17. Surface destruction of HO_2 is necessary to obtain high yields.

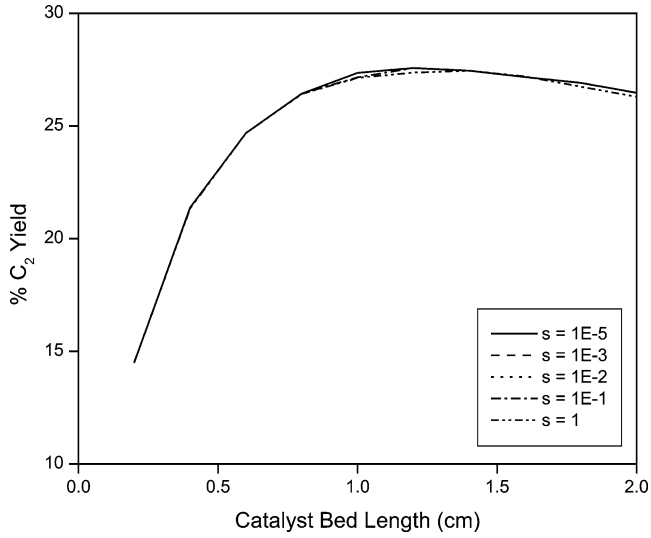

Fig. 11. Impact of $CH_3OO\cdot$ sticking coefficient on OCM C_2 yield bound. Modeling conditions: $\Delta H_{\text{abstraction}} = 125$ kJ/mol, $|\Delta H_{\text{adsorption}}| = 250$ kJ/mol, $T = 800\,^{\circ}\text{C}$, $P = 1$ atm, CH_4:O_2:N_2 feed ratio = 2:1:17. C_2 yields are not sensitive to changes in this sticking coefficient.

Upon observation of the significant impact of HO_2 on C_2 yield trajectories, the effects of CH_3OO quenching were also investigated. The major reaction channel in the gas phase for CH_3OO loss is $CH_3OO + CH_3 \rightarrow 2CH_3O$. Thus, it was suspected that the effective surface quenching of CH_3OO might also be necessary for high yields. As shown in Fig. 11, however, the computed C_2 yields are not sensitive to the CH_3OO sticking coefficient. At a sticking coefficient of unity, $\sim 72\%$ of CH_3OO destruction is due to surface reaction. HO_2 reacts more readily with the surface through an additional fast channel because of its weak O–H bond. Fortunately, because the concentration of CH_3OO is an order of magnitude less than that of HO_2, it has a negligible effect on the yield.

5. Conclusions

In this paper, we describe a simple approach for defining the inherent limits that may exist for a catalytic reaction. This approach allows for the coupling of our physical intuition about the catalyst's function with our knowledge of the elementary surface kinetics. Although the use of elementary steps to describe surface kinetics leads to a large number of reaction parameters, it allows us to operate within a thermodynamically consistent framework, which is critical. We have shown that scaling arguments can be used to reduce the dimensionality of the problem. For the remaining unknowns, we can turn to experimental data to establish a range of possible values for them. Thus, a methodical survey of the attainable yield becomes tractable.

Unlike previous modeling attempts to determine optimal catalytic performance, this methodology focuses on the catalyst's impact on the attainable yield. Oftentimes, in employing a surface mechanism fit using experimental data from a single catalyst, the unique behavior of that catalyst is downplayed. Optimization is conducted solely with respect to reactor parameters such as space-time, feed ratio, and temperature. Lost in this process is the key role of the catalyst surface kinetics on yields. Our results for OCM reaffirm the importance and uniqueness of catalyst behaviors in determining yields. This is demonstrated by the limited range of abstraction and adsorption enthalpies that correspond with superior catalytic performance.

In selecting OCM as a case study for this approach, our goal was to take into account additional complexities and perhaps more rigorously confirm Labinger's conclusion that OCM could not be economically feasible. OCM highlights some of the challenges encountered in attempting to obtain a high-yield catalyst, while providing a relatively simple and well-understood surface mechanism. Here, an upper bound of 28% for C_2 yield is determined for a continuous, CH_4/O_2 co-fed, single-pass process under conventional conditions used for catalyst screening. As Labinger and Ott [12,13] pointed out, the attainable yield computed under these laboratory conditions of diluted feed stream and atmospheric pressure is higher than that achievable at more realistic industrial conditions. Based on these results, it seems that existing catalysts are already close to the performance limit, and it does not appear that OCM can be viable with current economics [2–4] using a simple packed bed of catalyst that reacts via the conventional Eley–Rideal mechanism.

It remains to be seen how well real catalysts can be tailored to approach optimal surface thermochemistries. While it is difficult for the performance of idealized catalysts to be matched, this method does provide a guide to future catalyst development. We have found that a particular surface thermochemical behavior is a necessary requirement for

high OCM yield. Moreover, we have identified those specific combinations of enthalpies that result in optimal OCM behavior. With the growing interest in high-throughput catalyst screening, efficient metrics for identifying potentially superior catalysts are critical. In the case of OCM, for each new catalyst synthesized, adsorption and abstraction enthalpies may be measured to see whether they lie in the range where high yield may potentially exist. Thus, this simple metric for catalyst screening established for OCM should be very helpful for future studies.

Acknowledgments

This work was financially supported by Alstom Power. We thank C.A. Mims for his aid in securing the gas-phase reaction mechanism used in these studies.

Appendix A. Calculation of surface reaction enthalpies

The reactions involved in the main catalytic cycle of OCM are

$$O_2 + 2V^* \leftrightarrow 2O^*, \quad \Delta H_{ads}, \tag{A.1}$$

$$CH_4 + O^* \leftrightarrow CH_3 + OH^*, \quad \Delta H_{abs}, \tag{A.2}$$

$$OH^* + OH^* \leftrightarrow H_2O + O^* + V^*, \quad \Delta H_{recomb}, \tag{A.3}$$

$$CH_3 + CH_3 \leftrightarrow C_2H_6, \quad \Delta H_{coupling}.$$

The overall reaction is given by

$$2CH_4 + \tfrac{1}{2}O_2 \leftrightarrow C_2H_6 + H_2O, \quad \Delta H_{overall}.$$

$\Delta H_{overall}$ and $\Delta H_{coupling}$ involve only gas-phase species with well-known heats of formation. Upon independent fixing of reactions (A.1) and (A.2), the reaction enthalpy for reaction (A.3) is determined by

$$\Delta H_{recomb} = \Delta H_{overall} - \tfrac{1}{2}\Delta H_{ads} - 2\Delta H_{abs} - \Delta H_{coupling}.$$

We can then employ these values to specify surface species bond strengths, which are used to define enthalpies for the remaining surface reactions.

The formation of O^* species on the surface ($\Delta H_{M\text{–}O}$) is defined via reaction (A.1). This involves the dissociative adsorption of oxygen on the surface, the result of which is the formation of two active O^* species.

$$\Delta H_{M\text{–}O} = (\Delta H_{ads} - BDE_{O_2})/2,$$

where BDE_{O_2} is simply the bond dissociation energy of O_2 in the gas phase at the reaction temperature of interest. The energy associated with the transformation of V^* to OH^* ($\Delta H_{M\text{–}OH}$) can be defined by

$$\Delta H_{M\text{–}OH} = \Delta H_A + \Delta H_B - \Delta H_{abs} - \Delta H_{recomb},$$

where ΔH_A and ΔH_B are known enthalpies associated with the reactions

$$H + OH \leftrightarrow H_2, \quad \Delta H_A,$$

$$CH_4 \leftrightarrow CH_3 + H, \quad \Delta H_B.$$

Once $\Delta H_{M\text{–}OH}$ was defined, $\Delta H_{M\text{–}OCH_3}$ was scaled relative to it. As a first approximation,

$$\Delta H_{M\text{–}OCH_3} = \Delta H_{M\text{–}OH} + X_1,$$

where $X_1 = 41$ kJ/mol, the average of the difference in bond energies between R–OH and R–OCH_3 for several hydrocarbon species.

Furthermore, taking into account bonds broken/formed in reaction (A.2), we can determine the energy associated with the formation of MOH from MO^* as

$$\Delta H_{MO\text{–}H} = -\Delta H_B + \Delta H_{abs}.$$

Likewise,

$$\Delta H_{MO\text{–}CH_3} = \Delta H_{M\text{–}OCH_3} - BDE_{CH_3\text{–}O} - \Delta H_{M\text{–}O},$$

where $BDE_{CH_3\text{–}O}$ is the bond dissociation energy of methoxy radical.

As labeled in Table 1, the reaction enthalpies of reactions (4)–(7) were computed using the previously fixed value of ΔH_{abs},

$$\Delta H_{4\text{–}7} = \Delta H_{abs} - (BDE_{CH_3\text{–}H} - BDE_{R\text{–}H}),$$

where R–H represents the major products C_2H_6, C_2H_4, CH_2O, and CH_3OH.

Reaction (8), the first of four peroxy quenching reactions, was calculated via

$$\Delta H_8 = \Delta H_C + \Delta H_{MO\text{–}H},$$

where ΔH_C is the reaction enthalpy associated with

$$HO_2 \leftrightarrow O_2 + H, \quad \Delta H_C.$$

Reaction (9) is calculated as

$$\Delta H_9 = \Delta H_D + \Delta H_{M\text{–}O},$$

where ΔH_D is the reaction enthalpy associated with

$$HO_2 \leftrightarrow OH + O, \quad \Delta H_D.$$

Reaction (10) involves the reaction of surface vacancies in quenching gas-phase methyl peroxy radicals. The barrier for this reaction is defined by

$$\Delta H_{10} = BDE_{CH_3O\text{–}O} + \Delta H_{M\text{–}OCH_3} + \Delta H_{M\text{–}O},$$

where $BDE_{CH_3O\text{–}O}$ is the energy associated with breaking the O–O bond in CH_3OO. Reaction (11) is calculated as

$$\Delta H_{11} = BDE_{CH_3O\text{–}O} + \Delta H_{M\text{–}O}.$$

To define the reaction enthalpies associated with the hypothesized methyl radical degradation route on the surface,

we have

$$\Delta H_{12} = \Delta H_{\mathrm{MO–CH_3}}.$$

This is followed by further hydrogen abstraction from the resulting surface methoxy species. This abstraction can occur by gas-phase radicals, wherein the resulting reaction enthalpy may be described by

$$\Delta H_{13} = -\Delta H_{\mathrm{M–OCH_3}} + \Delta H_{\mathrm{E}} + \Delta H_{\mathrm{F}},$$

where ΔH_{E} is the enthalpy associated with the reaction

$$\mathrm{X} + \mathrm{H} \leftrightarrow \mathrm{XH}, \quad \Delta H_{\mathrm{E}}$$

and ΔH_{F} represents the reaction enthalpy of

$$\mathrm{OCH_3} \leftrightarrow \mathrm{OCH_2} + \mathrm{H}, \quad \Delta H_{\mathrm{F}}.$$

Here, we assume that the interaction between the surface and the resulting surface formaldehyde species is negligible. Alternatively, hydrogen abstraction from the surface methoxy can occur via neighboring surface oxygen species, at which point the enthalpy of reaction becomes

$$\Delta H_{14} = -\Delta H_{\mathrm{M–OCH_3}} + \Delta H_{\mathrm{MO–H}} + \Delta H_{\mathrm{F}}.$$

The resulting surface formaldehyde species simply desorb from the surface.

References

[1] H.S. Fogler, Elements of Chemical Reaction Engineering, Prentice–Hall, Englewood Cliffs, NJ, 1992.
[2] G.D. Tomlinson, Direct methane conversion—an assessment, Contractor Report, SAND-88-7110, 1988.
[3] S. Field, S.C. Niruta, J.G. McCarthy, SRI International, Project Report 6: 9129-01-SQ, 1989.
[4] M.J. Gradassi, N.W. Green, Fuel Proc. Technol. 42 (1995) 65.
[5] G.E. Keller, M.M. Bhasin, J. Catal. 73 (1982) 9.
[6] Y. Jiang, I.V. Yentekakis, C.G. Vayenas, Science 264 (1994) 1563.
[7] I.P. Androulakis, S.C. Reyes, AIChE J. 45 (1999) 860.
[8] A.J. Colussi, V.T. Amorebieta, J. Catal. 169 (1997) 301.
[9] P.M. Couwenberg, Q. Chen, G.B. Marin, Ind. Eng. Chem. Res. 35 (1996) 3999.
[10] M. Feinberg, D. Hildebrandt, Chem. Eng. Sci. 52 (1997) 1637.
[11] M. Feinberg, P. Ellison, Ind. Eng. Chem. Res. 40 (2001) 3181.
[12] J.A. Labinger, Catal. Lett. 1 (1988) 371.
[13] J.A. Labinger, K.C. Ott, J. Phys. Chem. 91 (1987) 2682.
[14] P.M. Couwenberg, Q. Chen, G.B. Marin, Ind. Eng. Chem. Res. 35 (1996) 415.
[15] C.A. Mims, R. Mauti, A.M. Dean, K.D. Rose, J. Phys. Chem. 98 (1994) 13357.
[16] D. Wolf, M. Slinko, E. Kurkina, C. Baerns, Appl. Catal. A 166 (1998) 47.
[17] J.S.J. Hargreaves, G.J. Hutchings, R.W. Joyner, Nature 348 (1990) 428.
[18] C. Shi, M.P. Rosynek, J.H. Lunsford, J. Phys. Chem. 98 (1994) 8371.
[19] M. Sinev, G.A. Vorobieva, V.N. Korchak, Kinet. Katal. 27 (1986) 1007.
[20] D.J.C. Yates, N.E. Zlotin, M. Hatano, P.G. Hinson, K.S. Vines, J.H. Lunsford, J. Catal. 124 (1990) 557.
[21] J.C. Mackie, J.G. Smith, P.F. Nelson, R.J. Tyler, Energy Fuel 4 (1990) 277.
[22] S. Lacombe, C. Geantet, C. Mirodatos, J. Catal. 151 (1995) 439.
[23] C. Li, K. Domen, K. Maruya, T. Onishi, J. Catal. 125 (1990) 445.
[24] T.-J. Yang, J.H. Lunsford, J. Catal. 103 (1987) 55.
[25] G.A. Somorjai, Chemistry in Two Dimensional Surfaces, Cornell University Press, Ithaca, NY, 1981.
[26] Y. Tong, J.H. Lunsford, J. Am. Chem. Soc. 113 (1991) 4741.
[27] Y.P. Arnaud, Appl. Surf. Sci. 62 (1992) 37.
[28] J.H. Lunsford, in: E.E. Wolf (Ed.), Methane Conversion by Oxidative Processes, Van Nostrand Reinhold, New York, 1994, p. 3.
[29] R.J. Gillespie, D.A. Humphreys, N.C. Baird, E.A. Robinson, Chemistry, 2nd ed., Allyn and Bacon, Inc., Needham Heights, MA, 1989.
[30] R.J. Kee, F.M. Rupley, J.A. Miller, M.E. Coltrin, J.F. Grcar, E. Meeks, H.K. Moffat, A.E. Lutz, G. Dixon-Lewis, M.D. Smooke, J. Warnatz, G.H. Evans, R.S. Larson, R.E. Mitchell, L.R. Petzold, W.C. Reynolds, M. Caracotsios, W.E. Stewart, P. Glarborg, C. Wang, O. Adigun, CHEMKIN Collection, Release 3.6, Reaction Design, Inc., San Diego, CA, 2000.
[31] M.E. Coltrin, R.J. Kee, J.A. Miller, J. Electrochem. Soc. 131 (1984) 425.
[32] M.E. Coltrin, R.J. Kee, J.A. Miller, J. Electrochem. Soc. 133 (1986) 1206.
[33] M.H. Abbasi, J.W. Evans, I.S. Abramson, AIChE J. 29 (1983) 617.
[34] S.S. Reyes, E. Iglesia, J. Catal. 129 (1991) 457.
[35] Z.S. Andrianova, A.N. Ivanova, P.E. Matkovskii, G.P. Startseva, Kinet. Katal. 37 (1996) 246.
[36] C.T. Campbell, J. Catal. 204 (2001) 520.
[37] J.A. Dumesic, J. Catal. 185 (1999) 496.
[38] K. Campbell, H. Zhang, J. Lunsford, J. Phys. Chem. 92 (1988) 750.
[39] S. Korf, J. Roos, W. Derksen, J. Vreeman, J.V. Ommen, J. Ross, Appl. Catal. 59 (1990) 291.